Mapping gaseous dimethylamine, trimethylamine, ammonia, and their particulate counterparts in marine atmospheres of China's marginal seas: Part 1 - Differentiating marine emission from continental transport

Dihui Chen[1], Yanjie Shen[1], Juntao Wang[1], Yang Gao[1,2], Huiwang Gao[1,2], Xiaohong Yao[1,2*]

[1]Key Laboratory of Marine Environment and Ecology, and Frontiers Science Center for Deep Ocean Multispheres and Earth System, Ministry of Education, Ocean University of China, Qingdao 266100, China
[2]Laboratory for Marine Ecology and Environmental Science, Qingdao National Laboratory for Marine Science and Technology, Qingdao 266237, China

[*]*correspondence to*: Xiaohong Yao (xhyao@ouc.edu.cn)

Abstract. To study sea-derived gaseous amines, ammonia, and primary particulate aminium ions in the marine atmosphere of China's marginal seas, an onboard URG-9000D Ambient Ion Monitor-Ion chromatography (AIM-IC, Thermo Fisher) was set up on the front deck of the R/V Dongfanghong 3 to semi-continuously measure the spatiotemporal variations in the concentrations of atmospheric trimethylamine (TMA_{gas}), dimethylamine (DMA_{gas}), and ammonia (NH_{3gas}) along with their particulate matter ($PM_{2.5}$) counterparts. In this study, we differentiated marine emissions of the gas species from continental transport using data obtained from December 9 to 22, 2019 during the cruise over the Yellow and Bohai seas, facilitated by additional short-term measurements collected at a coastal site near the Yellow Sea during summer, fall, and winter of 2019. The data obtained from the cruise and coastal sites demonstrated that the observed TMA_{gas} and protonated trimethylamine ($TMAH^+$) in $PM_{2.5}$ over the Yellow and Bohai seas overwhelmingly originated from marine sources. During the cruise, no significant correlation (P>0.05) was observed between the simultaneously measured $TMAH^+$ and TMA_{gas} concentrations. Additionally, the concentrations of $TMAH^+$ in the marine atmosphere varied around 0.28 ± 0.18 µg m^{-3} (average $\pm$ standard deviation), with several episodic hourly average values exceeding 1 µg m^{-3}, which were approximately one order of magnitude larger than those of TMA_{gas} (approximately 0.031 ± 0.009 µg m^{-3}). Moreover, there was a significant negative correlation (P<0.01) between the concentrations of $TMAH^+$ and NH_4^+ in $PM_{2.5}$. Therefore, the observed $TMAH^+$ in $PM_{2.5}$ was overwhelmingly derived from primary sea-spray aerosols. Using TMA_{gas} and $TMAH^+$ in $PM_{2.5}$ as tracers for sea-derived

basic gases and sea-spray particulate aminium ions, the values of non-sea-derived DMA_{gas}, and NH_{3gas}, and non-sea-spray particulate $DMAH^+$ in $PM_{2.5}$ were estimated. The estimated average values of each species contributed to 16%, 34%, and 65% of the observed average concentrations for non-sea-derived DMA_{gas}, NH_{3gas} and non-sea-spray particulate $DMAH^+$ in $PM_{2.5}$, respectively. Uncertainties remained in the estimations, as $TMAH^+$ may decompose into smaller molecules in seawater to varying extents. The non-sea-derived gases and non-sea-spray particulate $DMAH^+$ likely originated from long-range transport from the upwind continents based on the recorded offshore winds and increased concentrations of non-sea-salt SO_4^{2-} (nss-SO_4^{2-}) and NH_4^+ in $PM_{2.5}$. The lack of a detectable increase in particulate $DMAH^+$, NH_4^+, and nss-SO_4^{2-} concentrations in several SO_2 plumes did not support the secondary formation of particulate $DMAH^+$ in the marine atmosphere.

Keywords: Marine atmospheric NH_3, trimethylamine, dimethylamine, particulate aminium, sea-spray aerosol

1. Introduction

Gaseous amines and their particulate counterparts are vital for reduced nitrogen compounds in the marine atmosphere (Facchini et al., 2008; Müller et al., 2009; Hu et al., 2015; Hu et al., 2018; van Pinxteren et al., 2015; van Pinxteren et al., 2019; Yu et al., 2016; Xie et al., 2018; Zhou et al., 2019) and are primarily derived from seawater, where glycine betaine (GBT), trimethylamine N-oxide (TMAO), and choline are the three major precursors (Burg and Ferraris, 2008; Lidbury et al., 2015a; Lidbury et al., 2015b; Jameson et al., 2016; Taubert et al., 2017). GBT, TMAO, and choline are critical for maintaining the osmotic pressure in marine organisms. When released into the environment, they can be degraded by bacteria to trimethylamine (TMA), dimethylamine (DMA), or methylamines (MA) (Lidbury et al., 2015a; Lidbury et al., 2015b). Gaseous DMA, TMA, and MA may be vital in the formation of secondary particles in the atmosphere by nucleation (Almeida et al., 2013; Chen et al., 2016; Yao et al., 2018; Zhu et al., 2019). In addition to biogenic amines, anthropogenic emissions are known as important sources of amines in the continental atmosphere, but not in the marine atmosphere (Ge et al., 2011). Modeling studies have shown that the continental amine species in gas and/or particle phases can be transported regionally, including downwind marine atmospheres (Yu and Luo, 2014; Mao et al., 2018). Simultaneous real-time

measurement of gaseous amines and their particulate counterparts in the marine atmosphere over the ocean remains challenging because of artifact signals related to self-vessel emissions and amine-contained dew evaporation; however, this is not the case in the continental atmosphere (VandenBoer et al., 2011). The lack of direct measurements restricts the determination of their sources and the relationship between the reduced nitrogen compounds and acid-base neutralization reactions in the marine atmosphere.

Reduced nitrogen compounds in the ocean can finally decompose into ammonium ions (NH_4^+) and other smaller molecules. NH_4^+ in surface seawater releases to the marine atmosphere as atmospheric ammonia (NH_{3gas}) under favorable conditions (Johnson et al., 2008; Carpenter et al., 2012; Paulot et al., 2015). The ocean is an important source of NH_{3gas}, contributing to approximately 40% of the natural NH_3 emissions on Earth (Carpenter et al., 2012; Paulot et al., 2015). In the literature, large uncertainties remain in estimating NH_3 emissions from the ocean; for example, the annual emission flux ranges from 2 to 23 Tg N a^{-1} (Clarke and Porter, 1993; Dentener and Crutzen, 1994; Sutton et al., 2013; Paulot et al., 2015). These uncertainties are primarily derived from two factors: 1) the major marine sources of NH_{3gas} are still disputed, such as seawater, sea birds, or the photolysis of marine organic nitrogen at the ocean surface or in the atmosphere; and 2) direct NH_{3gas} observations in marine atmospheres are restricted as onboard ambient NH_{3gas} measurement techniques sometimes suffer from large artifacts from NH_{3gas} contamination associated with onboard human activities, dew evaporation, and water vapor interference (Quinn et al., 1990; Clarke and Porter, 1993; Johnson et al., 2008; Keene et al., 2009; Wentworth et al., 2016; Teng et al., 2017). Additionally, the long-range transport of atmospheric NH_{3gas} from the continent may also complicate the source analysis of NH_{3gas} in marine atmospheres (McNaughton et al., 2004; Uematsu et al., 2004; Zhao et al., 2015; Lutsch et al., 2016).

To identify and characterize sea-derived gaseous amines, ammonia, and sea-spray particulate aminium ions, as well as secondary particulate aminium ions from continental transport in the atmospheres of China's marginal seas, we conducted two cruise campaigns: one over the Yellow and Bohai seas in China from December 9 to 22, 2019 (Campaign A), and another over the Eastern China and Yellow seas from December 27, 2019 to January 16, 2020 (Campaign B). Winter cruise campaigns provide great opportunities for observational studies due to the following: 1) higher concentrations of nutrients in the seas at lower sea surface water temperatures, which may favor higher primary production (Guo et al., 2020) and subsequently increase marine emissions of gaseous amines and/or aminum-contained sea-spray aerosols; 2) periodically

enhanced air-sea exchanges driven by the strong winter Asian monsoon every 4–10 days (Zhu et al., 2018); and 3) periodically enhanced long-range transport of anthropogenic pollutants from continents to the seas, which may enhance the formation of secondary ammonium and aminium aerosols (Guo et al., 2016; Yu et al., 2016; Xie et al., 2018; Wang et al., 2019).

In this study, an onboard URG-9000D Ambient Ion Monitor-Ion chromatography (AIM-IC, Thermo Fisher) instrument was used to simultaneously measure the spatiotemporal variations in the concentrations of gaseous amines and NH_{3gas}, along with their counterparts in $PM_{2.5}$. Semi-continuous measurement data were analyzed to identify the study targets. This study was divided into two parts. In this section, we distinguish the marine sources from the continental transport of reduced nitrogen compounds in marine atmospheres and subsequently quantify each contribution to the observed species during the December 9-22, 2019 campaign. In the companion paper (Gao et al., 2021), we analyzed the spatiotemporal heterogeneity and related causes, and subsequently delivered a hypothesis regarding the marine emissions of reduced nitrogen compounds using the data from the two campaigns and an additional cruise campaign previously reported by Hu et al. (2015).

2. Experimental

2.1 Sampling periods, locations, and instruments

Campaign A was conducted from December 9 to 19, 2019 on the R/V Dongfanghong-3 with a displacement tonnage of 5000. The research vessel was still within its testing period and used state-of-the-art combustion technology with low-sulfur diesel. Campaign B started from December 27, 2019 to January 17, 2020, and was organized by another research team. During December 20-22, the vessel was anchored at the port while the sampling continued. The 44 hours were referred to as the transition period between campaigns A and B. A standard-sized air-conditioned container was set up on the front deck to house a suite of instruments including the AIM-IC, a fast-mobility particle sizer (FMPS, Tsi), a cloud condensation nuclei counter (CCN-100, Droplet MT), and a single particle aerosol mass spectrometer (SPAMS 05, Hexin). No human activities occurred on the front deck during cruising, excluding anchoring at the port. Even during the anchoring period, human activity on the front deck was rare. The use of the container on the front deck effectively minimized the self-vessel contamination by NH_{3gas} and gaseous amines. The front deck was approximately 10 m above sea level, and the container

height was 2.8 m.

To ensure that the onboard AIM-IC was operated properly, it was housed in a mobile air-conditioned mini-container, which was further placed in a standard container with a 1 m stainless steel sampling probe connected to the ambient air. The inlet of the sampling probe extended from the top corner of the standard container facing the sea. The AIM-IC consists of two major parts: an ambient air sampling system and an ion chromatography analysis system. For the sampling system, the AIM-IC was equipped with a $PM_{2.5}$ cyclone and operated at a rate of 3 L/min. The sampled gases and particles in the water solution were stored in two syringes prior to their injection for analysis. The ion chromatography analysis system measured the semi-continuous concentrations of chemically reactive gases. These included NH_{3gas}, gaseous amines, and acidic gases such as SO_2 and HNO_3, along with their particulate counterparts, at a temporal resolution of 1 h. This facilitated the identification of possible interference from onboard dew evaporation, which typically occurs with sunrise (Teng et al., 2017).

An automatic weather system providing real-time meteorological data is available on the R/V Dongfanghong-3. The heading wind was corrected to determine the true wind speed and direction. The surface seawater temperature was not measured during this cruise campaign, and typically had a delay of a few hours compared to the ambient air temperature (Deng et al., 2014).

On August 1-9, September 12 to October 1, and November 16 to December 1, 2019, the AIM-IC was set up at a coastal site in Qingdao (36.34° N, 120.67° E) to conduct routine measurements (Fig. 1). Coastal measurement data were obtained from two weeks to four months before the winter cruise campaign. The sampling site was located in a new high-technology zone near the Yellow Sea, with the shortest distance from the sea being approximately 1 km in the south. The AIM-IC was housed in a research lab on the fifth floor of a building, approximately 16 m above ground level. The sampling probe extended out of the window and was directly connected to the ambient air. Typically, higher biogenic emissions of reduced nitrogen compounds over the continents are expected in the summer than in the winter owing to the temperature effect (Yu et al., 2016; Teng et al., 2017).

2.2 Chemical analysis

The AIM-IC includes an ICS-1100 ion chromatograph, wherein an analytical column (Ion Pac CS17A (2×250 mm)) was

used to measure cations, including Na^+, NH_4^+, protonated dimethylamine ($DMAH^+$), and protonated trimethylamine ($TMAH^+$), and an AS11-HC (2×50 mm) was used to measure anions, including SO_4^{2-}, NO_3^-, Cl^-, and organic ions. Methanesulfonic acid solution (5 mM) was used as the eluent for cation analysis, while potassium hydroxide solution (varying from 3 to 40 mM) was used as the gradient eluent for anion analysis. Each analysis took 26-28 mins to obtain a complete ion spectrum. The volume of the injection loop installed on the low-pressure valve was 250 μL, which substantially reduced the limits of detection for all ions. The limits of detection for NH_4^+, $DMAH^+$, and $TMAH^+$ were 0.0004, 0.004, and 0.002 μg m^{-3}, respectively, in ambient air. The limits of detection for NO_3^- and SO_4^{2-} were 0.05 and 0.015 μg m^{-3}, respectively, in ambient air. The ICS-1100 was calibrated onboard prior to obtaining regular measurements, and the second calibration was conducted when the vessel was anchored at the port. The AIM-IC analysis was not affected by ambient water vapor, as the device directly measured the ions. Detailed information regarding the AIM-IC analysis is provided in Teng et al. (2017) and Xie et al. (2018). Notably, strong K^+ interference occurred unexpectedly and occasionally, and then disappeared during different campaigns. When the interference occurred, $DMAH^+$ and $TMAH^+$ were undetectable because of the increased baseline at the corresponding residence time in the ion chromatograph (Fig. S1); consequently, some $PM_{2.5}$ $DMAH^+$ and $TMAH^+$ concentration data are unavailable in Fig. 1. However, the concentrations of gaseous amines were still detected correctly, with a low baseline at the residence. K^+ interference remains to be investigated. Additionally, a few surface seawater samples were collected from different sea zones. The NH_4^+ and aminium ion concentrations in the samples were not measured, as the analytical methods were still hindered by high sea-salt ion contents.

3. Results

3.1 Temporal variations in the concentrations of basic gases and their $PM_{2.5}$ counterparts in the coastal atmosphere

Before analyzing the basic gases and their counterparts in the marine atmosphere, we initially presented their continental concentrations at the coastal site facing the Yellow Sea as important evidence to facilitate the analysis of the contributors to these species in the marine atmosphere. Figs. 1a & b show that the TMA_{gas} and $TMAH^+$ concentrations in $PM_{2.5}$ were mostly below the detection limit, varying at approximately 0.001±0.001 μg m^{-3} (average ± standard deviation), regardless of the presence of offshore or onshore winds during short-term measurements in the three seasons of 2019. The DMA_{gas} and

DMAH$^+$ concentrations varied at 0.018±0.021 and 0.017±0.013 μg m^{-3}, respectively, which were approximately one order of magnitude larger than those of TMA$_{gas}$ and TMAH$^+$. TMA$_{gas}$ and TMAH$^+$ concentrations in the upwind continental and coastal atmospheres were substantially lower than those reported in the literature, by up to a few tens of ng m^{-3} (Ge et al., 2011). However, Gibb et al. (1999) reported a low average TMA$_{gas}$ (0.5 ng m^{-3}) and particulate TMAH$^+$ (0.5 ng m^{-3}) in the marine atmosphere over the Arabian Sea on November 16 to December 19, 1994. Xie et al. (2018) reported that TMAH$^+$ concentrations were comparable to those of DMAH$^+$ in atmospheric particles collected at two other coastal sites located approximately 20 km from the study area, as listed in Table S1. The cause of this change is beyond the scope of this study, but may be due to the large decrease in manure application, based on our recent survey in the Qingdao area.

The DMA$_{gas}$ and DMAH$^+$ concentrations in PM$_{2.5}$ with offshore winds from the north were substantially higher than those with onshore winds from the south or southeast (top of Fig. 1a), suggesting that their continental emissions and related secondary sources were stronger. Moreover, the concentrations of DMA$_{gas}$ and DMAH$^+$ were moderately correlated with those of NH$_{3gas}$ and NH$_4^+$; namely, [DMA$_{gas}$] = $5.6 \times 10^{-3} \times$ [NH$_{3gas}$] (R^2=0.79, P<0.01), and [DMAH$^+$]$_{PM2.5}$=$5.9 \times 10^{-3} \times$ [NH$_4^+$]$_{PM2.5}$ (R^2=0.84, P<0.01). Generally, the DMA$_{gas}$ and DMAH$^+$ concentrations were approximately 1/200 of those of the corresponding NH$_{3gas}$ and NH$_4^+$.

3.2 Spatiotemporal variations in the concentrations of basic gases over the seas

Throughout Campaign A, the TMA$_{gas}$ concentrations varied at approximately 0.031±0.009 μg m^{-3} (Figs. 2a-c), with three peaks occurring at 4–5 day intervals (gray shadowing in Fig. 2c). Peaks 1 and 2 were generally associated with offshore winds, while peak 3 was mostly associated with onshore winds (Fig. 2b). The peaks lasted from tens to dozens of hours and were not induced by the onboard dew evaporation at sunrise. For example, the highest value (0.060 μg m^{-3}) occurred at 23:00 on December 16. The observed TMA$_{gas}$ concentrations were one order of magnitude higher than those measured in the coastal atmosphere during the summer, fall, and winter. This suggested that the TMA$_{gas}$ observed during Campaign A was largely derived from marine sources rather than from long-range continental transport. The same conclusion can be drawn by analyzing the three peaks of TMA$_{gas}$ and its temporal variations during the anchoring port period. For example, during peak 1 (Fig. 2a), the concentrations of TMA$_{gas}$ increased by approximately 100% from 20:00 on December 9 to 11:00 on

December 10, with an approximately 30% decrease in the non-sea-salt SO_4^{2-} (nss-SO_4^{2-}) concentration (from 22 to 16 μg m^{-3}; Fig. 2b). Moreover, the peaks in the TMA_{gas} concentrations corresponded to troughs in the nss-SO_4^{2-} concentrations during peak 3, as shown in Figs. 2c & d. The self-vessel emissions of nss-SO_4^{2-} in $PM_{2.5}$ were negligible because of the use of low-sulfur diesel, which is discussed later. The increased nss-SO_4^{2-} concentrations in $PM_{2.5}$ may be a good indicator of continental transport, and vice versa.

The concentrations of DMA_{gas} varied at approximately 0.006±0.006 μg m^{-3} (Fig. 2d) and were significantly higher than those of TMA_{gas} (P<0.01). Unlike TMA_{gas}, continental transport was likely an important contributor to the DMA_{gas} and NH_{3gas} observed in the marine atmosphere, particularly during peak 1, when higher nss-SO_4^{2-} concentrations were observed in $PM_{2.5}$ (Figs. 2c-e). The DMA_{gas} and NH_{3gas} concentrations were negatively correlated with those of TMA_{gas} during peak 1; namely, R^2=0.35 (P<0.01) between TMA_{gas} and DMA_{gas}, and R^2=0.17 (P<0.01) between TMA_{gas} and NH_{3gas}. This suggested that most of the DMA_{gas} and NH_{3gas} were likely derived from continental transport, rather than marine sources. During peak 2, increased TMA_{gas}, DMA_{gas}, and NH_{3gas} concentrations were concurrently observed with increasing nss-SO_4^{2-} concentrations, suggesting that both marine emissions and continental transport simultaneously contributed to the observed DMA_{gas} and NH_{3gas}. During the port-anchoring period from December 20-22, the DMA_{gas} and NH_{3gas} concentrations varied slightly, and were moderate and low, respectively. However, the TMA_{gas} concentrations continuously increased by over 100% as the ambient temperature increased (Figs. 2c and f). Additionally, the nss-SO_4^{2-} concentrations of $PM_{2.5}$ varied greatly and followed a bell-shaped pattern during the port-anchoring period.

Additionally, the NH_{3gas} concentrations varied at approximately 0.53 ± 0.53 μg m^{-3} from December 9-22. The variation narrowed to approximately 0.24 ± 0.07 μg m^{-3} during the port-anchoring period from December 20-22. When the data during Campaign A were used for the analysis, the NH_{3gas} concentrations were significantly correlated with those of DMA_{gas}; namely, $[DMA_{gas}] = 9.2\times10^{-3} \times [NH_{3gas}]$ (R^2=0.71, P<0.01). However, there was no correlation between NH_{3gas} and TMA_{gas} concentrations.

3.3 Spatiotemporal variations in the aminium and NH_4^+ ion concentrations of $PM_{2.5}$ over the seas

Figs. 3a-f show the spatiotemporal variations in the $TMAH^+$, $DMAH^+$, and NH_4^+ concentrations of $PM_{2.5}$ throughout

Campaign A from December 9-22, during which the $TMAH^+$ concentrations varied greatly at approximately 0.28 ± 0.18 µg m^{-3}. However, they narrowed at approximately 0.21 ± 0.04 µg m^{-3} during the port-anchoring period. The $TMAH^+$ concentrations generally increased from 0.13 ± 0.05 µg m^{-3} on December 9 to 0.46 ± 0.05 µg m^{-3} on December 16 (Fig. 3a), and subsequently decreased to approximately 0.2 µg m^{-3} thereafter, excluding some strong peaks from 0.62–1.24 µg m^{-3} at 03:00–05:59 and 1.02–1.81 µg m^{-3} at 14:00–16:59 on December 18 (grey shadowing representing peak 4 in Figs. 3a-d). The peaks reproduced the episodes observed in the marine atmosphere over the Yellow Sea in May 2012 (Hu et al., 2015) and were repeatedly observed during Campaign B (Gao et al., 2021). However, they were not observed in several other marine cruise campaigns conducted across the marginal seas of China and the northwestern Pacific Ocean (Hu et al., 2018; Xie et al., 2018).

As the $TMAH^+$ concentrations were approximately two orders of magnitude higher than those observed at the coastal site during the three seasons of 2019, the observed $TMAH^+$ was largely derived from marine sources. The $TMAH^+$ concentrations followed a spatiotemporal pattern that clearly differed from those of $DMAH^+$ and NH_4^+, while the latter two ions exhibited a similar spatiotemporal pattern during most periods of Campaign A (Figs. 3a-c). A significant negative correlation ($P<0.01$) was observed between the concentrations of $TMAH^+$ and NH_4^+ in $PM_{2.5}$ (not shown). The spatiotemporal pattern of the $TMAH^+$ concentration also significantly differed from those of nss-SO_4^{2-} (Fig. 2d) and SO_2 (Fig. 3b), which are regarded as tracers of long-range transported continental pollutants and fresh vessel plumes. For example, extremely strong $TMAH^+$ peaks occurred concurrently with low nss-SO_4^{2-}, NH_4^+, and SO_2 concentrations, accompanied by high Na^+ concentrations under high wind speeds, which are common indicators of sea spray aerosols (Feng et al., 2017). Moreover, the $TMAH^+$ concentrations were approximately one order of magnitude larger than those of TMA_{gas}, and no significant correlation was observed between them ($P>0.05$). This suggests that the observed $TMAH^+$ may not be derived from the neutralization reactions of TMA_{gas} with acids in the marine atmosphere, and may have been derived from primary sea-spray organic aerosols (Hu et al., 2015, 2018). Primary sea-spray organic aerosols mainly contain primary and degraded biogenic organics (Ault et al., 2013; Prather et al., 2013; Quinn et al., 2015; Dall'Osto et al., 2019).

The $DMAH^+$ concentrations varied at approximately 0.065 ± 0.068 µg m^{-3} from December 9-22; however, they varied at approximately 0.10 ± 0.04 µg m^{-3} during the port-anchoring period. The 25th percentile value of $DMAH^+$ during Campaign A

220 was 0.021 µg m^{-3}, suggesting a low background concentration in the marine area. The DMAH$^+$ concentrations were significantly correlated with those of NH$_4^+$ (R^2=0.71, P<0.01; data not shown). When the data obtained at 03:00–05:59 and 14:00–16:59 on December 18 (strong peaks of TMAH$^+$ with a simultaneous increase in DMAH$^+$) were removed for correlation, the R^2 value improved to 0.78. Unlike TMAH$^+$, the observed DMAH$^+$ may have been partially derived from acid-basic neutralization reactions in the ambient air, in addition to the primary sea-spray organic aerosols. For example, a

225 large increase in DMAH$^+$ concentrations occurred concurrently with strong peaks in the TMAH$^+$ concentrations (gray shadowed peak 4 in Figs. 3a & b).

The NH$_4^+$ concentrations of PM$_{2.5}$ varied greatly at approximately 4.7±7.2 µg m^{-3} during Campaign A (Fig. 3c). However, the 25th percentile values were as low as 0.21 µg m^{-3}, suggesting low marine background values. The 50th percentile value was also only 1.2 µg m^{-3}, which was considerably smaller than the average owing to the presence of strong peaks in NH$_4^+$

230 concentrations. The increased NH$_4^+$ concentrations associated with NO$_3^-$ and nss-SO$_4^{2-}$ during Campaign A were likely due to the long-range transport from the upwind continents.

4. Discussion

4.1 Effects of temperature on the observed basic gases in the marine atmosphere

As mentioned above, the observed TMA$_{gas}$ likely originated from marine sources. We plotted the concentrations of TMA$_{gas}$

235 against the ambient air temperature (T) in Fig. 4a, which generally increased with increasing T. We further separated the average hourly wind speeds (WS) into three categories: WS ≤ 5.0, 5.0 < WS ≤ 9.0, and WS > 9.0 m s^{-1}. At WS > 9.0 m s^{-1}, the data obtained from 15:00 on December 16 to 01:00 on December 19, including peaks 3 and 4, were separately considered as half-full symbols in Fig. 4a. The concentrations of TMA$_{gas}$ (half-full symbols) generally exceeded those of the other gases at the same T, with which they exhibited a moderately good exponent correlation ([TMA$_{gas}$] = 0.03 × e$^{0.04T}$ with R^2=0.72).

240 From 15:00 on December 16 to 01:00 on December 19, stronger emission potentials of TMA$_{gas}$ to the marine atmosphere were expected in the corresponding marine zone. However, the measured concentrations of TMAH$^+$ and seawater pH in surface seawater are required to confirm this.

Following the same approach, the DMA$_{gas}$ and NH$_{3gas}$ concentrations were plotted against T, as shown in Figs. 4b & c,

respectively. These values generally increased with increasing T. The NH_{3gas} concentrations (half-full symbols) were strongly correlated with T ($[NH_{3gas}] = 0.05 \times e^{0.3T}$ with $R^2=0.96$). As lower concentrations of nss-SO_4^{2-}, NH_4^+, and SO_2 were generally observed simultaneously, the continental transport of NH_{3gas} was greatly reduced; therefore, the observed NH_{3gas} was mainly derived from the seas. Therefore, the seas were the net source of NH_{3gas} at the time of measurement. However, at the same T, the NH_{3gas} concentrations (half-full symbols) were generally lower than those during other periods in this study. The concentrations of NH_4^+ in surface seawater may have been lower at the time of measurement. However, this may not be the case, as higher concentrations of $TMAH^+$ were expected. Alternatively, the continental transport of NH_{3gas} may have made an important contribution to the observed NH_{3gas} during most other periods when the seas were the net NH_{3gas} sink.

DMA_{gas} exhibited an extremely good exponent correlation with T (half-full symbols) at the measurement time ($[DMA_{gas}] = 0.001 \times e^{0.3T}$ with $R^2=0.91$). At the same T, the DMA_{gas} concentrations (half-full symbols) were not always higher or lower than the others. We considered these two hypotheses: In hypothesis 1, the observed DMA_{gas} concentrations exceeded those predicted by the regression equation using the ambient T as the input; the seas were the net sinks of DMA_{gas}. In hypothesis 2, including all others, measurements of $DMAH^+$ in the surface seawater were required to confirm whether the seas were net sources or sinks of DMA_{gas}.

4.2 Estimating the sea-derived DMA_{gas} and NH_{3gas} in the marine atmosphere

To estimate the sea-derived DMA_{gas} and NH_{3gas} concentrations in the marine atmosphere, we plotted the DMA_{gas} and NH_{3gas} concentrations against TMA_{gas}, as shown in Figs. 5a and b. The purple-red and dark-green markers represent the data obtained, with increasing concentrations of the three species from 10:00 on December 14 to 23:00 on December 16 (increasing period), and with decreasing concentrations from 23:00 on December 16 to 19:59 on December 17 (decreasing period) during peak 3, respectively; these were analyzed separately. A good correlation was obtained between DMA_{gas} and TMA_{gas} during the increasing period ($[DMA_{gas}] = 0.64 \times [TMA_{gas}] - 0.01$, $R^2=0.86$, and $P<0.01$). The good correlation suggested that DMA_{gas} was likely released with TMA_{gas} from the seawater and facilitated the estimation of non-sea-derived DMA_{gas} ($DMA_{gas}^{\#}$) concentrations using the regression equation. We assumed that any data beyond the purple-red dashed line reflected the non-sea-derived DMA_{gas}, which can be attributed to continental transport. Therefore, we assumed that the

DMA_{gas}# concentrations were equal to the observed values of DMA_{gas} minus the predicted values obtained using $[DMA_{gas}] = 0.64 \times [TMA_{gas}]$ - 0.01; the calculated DMA_{gas}# values are shown in Fig. 5c. During peak 1, the calculated DMA_{gas}# contributed to over 40% of the observed DMA_{gas} for 12 h. Similar calculated results for DMA_{gas}# were obtained during peak 2.

However, the equation for the decreasing period was as follows: $[DMA_{gas}] = 1.4 \times [TMA_{gas}]$ - 0.05, R^2=0.84, and P<0.01. The decreasing R^2 value and the increasing slope suggest that the $TMAH^+$ in the surface seawater may decompose into $DMAH^+$ to different extents (Lidbury et al., 2015a; Lidbury et al., 2015b; Xie et al., 2018). The two regression curves (purple-red and dark-green dashed lines in Figs. 5a and b) created a large triangular zone that likely reflected the different ratios of DMA_{gas}/TMA_{gas} in primary marine emissions on the cruise route. Based on the triangular zone in Fig. 5a, the aforementioned calculations should be considered as the lower limit of DMA_{gas}#.

The same approach was employed to analyze the NH_{3gas} results, as shown in Figs. 5b and d. During peak 1, the calculated non-sea-derived NH_{3gas} (NH_{3gas}#) contributed to over 40% of the observed NH_{3gas} for 17 h. During peak 2, the calculated NH_{3gas}# contributed to over 40% of the observed NH_{3gas} for 24 h.

Overall, the DMA_{gas}# and NH_{3gas}# concentrations varied at approximately 0.001±0.002 and 0.18±0.39 μg m^{-3}, respectively. The calculated average DMA_{gas}# and NH_{3gas}# values accounted for 16% and 34% of the observed averages of each species, respectively. The estimations suggested an appreciable continental contribution to the observed DMA_{gas} and NH_{3gas} during Camping A.

4.3 Estimation of non-sea-spray particulate $DMAH^+$ in the marine atmosphere

We plotted the concentrations of $DMAH^+$ against those of $TMAH^+$ in $PM_{2.5}$ (Fig. 6a) using the data obtained from 15:00 on December 16 to 01:00 on December 19 ($[DMAH^+]_{PM2.5}$ =0.13 × $[TMAH^+]_{PM2.5}$, R^2=0.91, P<0.01). During this period, largely increased concentrations of $DMAH^+$ and $TMAH^+$ were observed under high wind speeds of 9-13 m s^{-1}. The good correlation suggested that the observed $DMAH^+$ was likely released with $TMAH^+$ as amines-contained sea spray aerosols in the atmosphere, and facilitated the calculation of sea-derived $DMAH^+$ using $TMAH^+$ as a tracer of sea-spray aerosols. Thus, the

non-sea-derived DMAH$^+$ concentrations in PM$_{2.5}$, marked as DMAH$^{+\#}$, were assumed to be equal to the observed DMAH$^+$ values minus the predicted values (sea-derived DMAH$^+$) using the regression equation. The calculated DMAH$^{+\#}$ values are shown in Fig. 6b. The DMAH$^{+\#}$ concentrations varied at approximately 0.042±0.070 µg m^{-3} throughout Campaign A, during which the calculated average DMAH$^{+\#}$ accounted for 65% of the observed average. Additionally, the calculated DMAH$^{+\#}$ values accounted for over 80% of the observed values in 26% of the Campaign A period. The estimations suggested that the observed DMAH$^+$ originated predominantly from long-range continental transport and/or secondary formation in the marine atmosphere. The analysis was supported by the good correlation between the concentrations of DMAH$^{+\#}$ and those of NH$_4^+$; namely, [DMAH$^{+\#}$]$_{PM2.5}$ = 0.0089× [NH$_4^+$]$_{PM2.5}$, (R^2=0.82, P<0.01; Fig. 6c). The slope of 0.0089 was approximately 50% larger than that obtained in the coastal atmosphere (0.0059), suggesting more DMA$_{gas}$ partitioning in PM$_{2.5}$ in the marine atmosphere than in the coastal atmosphere (Pankow, 2015; Xie et al., 2018).

Moreover, the decomposition of TMAH$^+$ to DMAH$^+$ may have occurred in surface seawater and/or the marine atmosphere, to an extent, and the estimated DMAH$^{+\#}$ should be considered as the upper limit. Notably, the NH$_4^+$ and TMAH$^+$ concentrations were negatively correlated during Campaign A, and no primary particulate NH$_4^+$ from sea-spray aerosols were identified.

4.4 Formation and chemical conversion of aminium ions in the transported and self-vessel SO$_2$ plumes

When the sea-spray particulate DMAH$^+$ was deducted, the increased concentrations of DMAH$^{+\#}$ were generally associated with increased nss-SO$_4^{2-}$ and SO$_2$ concentrations. Combining this with the moderate correlation between DMAH$^{+\#}$ and NH$_4^+$, we inferred that DMAH$^{+\#}$ likely originated from concurrent secondary formation with NH$_4^+$. However, we separated the air pollutant plumes into two groups. Group 1 represented an increase in nss-SO$_4^{2-}$ and NH$_4^+$ together with SO$_2$, while group 2 represented an increase in SO$_2$ without increases in nss-SO$_4^{2-}$ and NH$_4^+$. Group 1 likely reflected the transport of aged air pollutant plumes from the continents, while group 2 may reflect self-vessel SO$_2$ plumes. As shown in Figs. 6b and 3b-c, the concentrations of DMAH$^{+\#}$ and NH$_4^+$ in the self-vessel SO$_2$ plumes did not increase in the intervals between peaks 1 and 2 and between peaks 2 and 3. Therefore, no fresh formation of DMAH$^{+\#}$ and NH$_4^+$ in the self-vessel emissions was detected. However, the concentrations of TMAH$^+$ decreased in some self-vessel SO$_2$ plumes. The TMAH$^+$ concentrations were

approximately one order of magnitude higher than those of TMA_{gas} in the marine atmosphere. Assuming that the decreased $TMAH^+$ was released from $PM_{2.5}$ to the gas phase, a simultaneous large spike in TMA_{gas} should be observed. However, this was not the case, as shown in Fig. 1c. The decreased $TMAH^+$ may persist in $PM_{2.5}$, but could not be detected by AIM-IC.

5. Conclusion and Implication

320   In continental China upwind of the Yellow Sea, the TMA_{gas} and $TMAH^+$ concentrations in $PM_{2.5}$ were extremely low (0.001 ± 0.001 μg m^{-3}), mostly below the detection limit of the AIM-IC. Considering the observations as a reference, the largely increased TMA_{gas} (0.031 ± 0.009 μg m^{-3}) and particulate $TMAH^+$ (0.28 ± 0.18 μg m^{-3}) concentrations in the marine atmosphere were attributed to marine emissions. Therefore, TMA_{gas} and particulate $TMAH^+$ can be used as unique tracers to quantify the marine emissions of DMA_{gas}, NH_{3gas}, and particulate $DMAH^+$, as well as the long-range transport from upwind

325   continental China.

Through comprehensive comparison and correlation analyses, the high concentrations of $TMAH^+$ in $PM_{2.5}$ observed over the Yellow and Bohai seas, with episodic hourly averages exceeding 1 μg m^{-3}, were inferred to originate from strong primary sea-spray aerosol emissions. Moreover, the TMA_{gas} concentrations generally increased with increasing ambient temperature and sea surface wind speeds, suggesting that the observed TMA_{gas} was likely released from the surface seawater. However,

330   the TMA_{gas} concentrations were substantially lower than those of particulate $TMAH^+$, and were not significantly correlated. Although different mechanisms have been reported in the literature for the release of TMA_{gas} and particulate $TMAH^+$ from the seas, the lack of a significant correlation between them was surprising and was explored in the companion study.

The DMA_{gas} and NH_{3gas} concentrations varied at approximately 0.006 ± 0.006 and 0.53 ± 0.53 μg m^{-3} during Campaign A, wherein at least 16% and 34% of the observational values were derived from continental transport, respectively. The sea-

335   derived DMA_{gas} and NH_{3gas} were likely released with TMA_{gas} as they peaked simultaneously. The $DMAH^+$ concentrations in $PM_{2.5}$ varied at approximately 0.065 ± 0.068 μg m^{-3} during Campaign A, 65% of which was derived from continental transport.

Our analysis results did not support the occurrence of photolysis of marine organic nitrogen to generate NH_{3gas} in the marine atmosphere during winter, as there was no correlation between the sea-derived NH_{3gas} and particulate $TMAH^+$ concentrations.

340 Additionally, peaks 2 and 3 of NH_{3gas} persisted for dozens of hours under strong winds and were therefore unlikely to be derived from seabird emissions. A good exponent correlation was observed between the observed NH_{3gas} concentrations and T during the period without continental air pollutant transport, suggesting that the observed NH_{3gas} was released from seawater. NH_3 emissions from seabirds were unlikely contributors to the observed NH_{3gas} in the marine atmosphere during winter; however, this may not have been the case during other seasons.

345 Additionally, no formation of particulate NH_4^+ and $DMAH^+$ in the self-vessel SO_2 plume was observed in the marine atmosphere. However, the particulate $TMAH^+$ concentration clearly decreased in the self-vessel SO_2 plume without a simultaneous increase in the TMA_{gas} concentration. Chemical conversion of particulate $TMAH^+$ likely occurred in the plume, while AIM-IC could not detect the products. This requires further investigation.

Data availability. The data of this paper are available upon request (contact: Xiaohong Yao, xhyao@ouc.edu.cn).

350 **Acknowledgment**

This research is supported by the Natural Science Foundation of China (grant no. 41776086), the National Key Research and Development Program in China (grant no. 2016YFC0200504), the Fundamental Research Funds for the Central Universities (202072002).

References

355 Almeida, J., Schobesberger, S., Kürten, A., Ortega, I. K., Kupiainen-Määttä, O., Praplan, A. P., Adamov, A., Amorim, A., Bianchi, F., Breitenlechner, M., David, A., Dommen, J., Donahue, N. M., Downard, A., Dunne, E., Duplissy, J., Ehrhart, S., Flagan, R. C., Franchin, A., Guida, R., Hakala, J., Hansel, A., Heinritzi, M., Henschel, H., Jokinen, T., Junninen, H., Kajos, M., Kangasluoma, J., Keskinen, H., Kupc, A., Kurtén, T., Kvashin, A. N., Laaksonen, A., Lehtipalo, K., Leiminger, M., Leppä, J., Loukonen, V., Makhmutov, V., Mathot, S., McGrath, M. J., Nieminen, T., Olenius, T., Onnela,
360 A., Petäjä, T., Riccobono, F., Riipinen, I., Rissanen, M., Rondo, L., Ruuskanen, T., Santos, F. D., Sarnela, N., Schallhart, S., Schnitzhofer, R., Seinfeld, J. H., Simon, M., Sipilä, M., Stozhkov, Y., Stratmann, F., Tomé, A., Tröstl, J., Tsagkogeorgas, G., Vaattovaara, P., Viisanen, Y., Virtanen, A., Vrtala, A., Wagner, P. E., Weingartner, E., Wex, H.,

Williamson, C., Wimmer, D., Ye, P., Yli-Juuti, T., Carslaw, K. S., Kulmala, M., Curtius, J., Baltensperger, U., Worsnop, D. R., Vehkamäki, H., and Kirkby, J.: Molecular understanding of sulphuric acid–amine particle nucleation in the atmosphere, Nature, 502, 359–363, https://doi.org/10.1038/nature12663, 2013.

365

Ault, A. P., Moffet, R. C., Baltrusaitis, J., Collins, D. B., Ruppel, M. J., Cuadra-Rodriguez, L. A., Zhao, D., Guasco, T. L., Ebben, C. J., Geiger, F. M., Bertram, T. H., Prather, K. A., and Grassian, V. H.: Size-dependent changes in sea spray aerosol composition and properties with different seawater conditions, Environmental Science & Technology, 47, 5603–5612, https://doi.org/10.1021/es400416g, 2013.

Burg, M. B. and Ferraris, J. D.: Intracellular organic osmolytes: Function and regulation, Journal of Biological Chemistry, 283, 7309–7313, https://doi.org/10.1074/jbc.R700042200, 2008.

370

Carpenter, L. J., Archer, S. D., and Beale, R.: Ocean-atmosphere trace gas exchange, Chem. Soc. Rev., 41, 6473–6506, https://doi.org/10.1039/C2CS35121H, 2012.

Chen, H., Varner, M. E., Gerber, R. B., and Finlayson-Pitts, B. J.: Reactions of methanesulfonic acid with amines and ammonia as a source of new particles in air, The Journal of Physical Chemistry B, 120, 1526–1536, https://doi.org/10.1021/acs.jpcb.5b07433, 2016.

375

Clarke, A. D. and Porter, J. N.: Pacific marine aerosol: 2. Equatorial gradients in chlorophyll, ammonium, and excess sulfate during SAGA 3, J. Geophys. Res., 98, 16997–17010, https://doi.org/10.1029/92JD02481, 1993.

Dall'Osto, M., Airs, R. L., Beale, R., Cree, C., Fitzsimons, M. F., Beddows, D., Harrison, R. M., Ceburnis, D., O'Dowd, C., Rinaldi, M., Paglione, M., Nenes, A., Decesari, S., and Simó, R.: Simultaneous detection of alkylamines in the surface ocean and atmosphere of the Antarctic sympagic environment, ACS Earth and Space Chemistry, 3, 854–862, https://doi.org/10.1021/acsearthspacechem.9b00028, 2019.

380

Deng, Y., Gao, T., Gao, H., Yao, X., and Xie, L.: Regional precipitation variability in East Asia related to climate and environmental factors during 1979-2012, Sci Rep, 4, 5693, https://doi.org/10.1038/srep05693, 2014.

Dentener, F. J. and Crutzen, P. J.: A three-dimensional model of the global ammonia cycle, Journal of Atmospheric Chemistry, 19, 331–369, https://doi.org/10.1007/BF00694492, 1994.

385

Facchini, M. C., Decesari, S., Rinaldi, M., Carbone, C., Finessi, E., Mircea, M., Fuzzi, S., Moretti, F., Tagliavini, E.,

Ceburnis, D., and O'Dowd, C. D.: Important source of marine secondary organic aerosol from biogenic amines, Environmental Science & Technology, 42, 9116–9121, https://doi.org/10.1021/es8018385, 2008.

390   Feng, L., Shen, H., Zhu, Y., Gao, H., and Yao, X.: Insight into generation and evolution of sea-salt aerosols from field measurements in diversified marine and coastal atmospheres, Scientific Reports, 7, 41260, https://doi.org/10.1038/srep41260, 2017.

Gao, Y., Chen, D., Shen, Y., Gao, Y., Gao, H., and Yao, X.: Mapping gaseous amines, ammonia and their particulate counterparts in marine atmospheres of China's marginal seas: Part 2 - spatiotemporal heterogeneity, causes and
395   hypothesis, Atmos. Chem. Phys. Discuss. [preprint], https://doi.org/10.5194/acp-2021-301, in review, 2021.

Gibb, S. W., Mantoura, R. F. C., and Liss, P. S.: Ocean-atmosphere exchange and atmospheric speciation of ammonia and methylamines in the region of the NW Arabian Sea, Global Biogeochemical Cycle, 13, 161–178, https://doi.org/10.1029/98GB00743, 1999.

Guo, C., Zhang, G., Sun, J., Leng, X., Xu, W., Wu, C., Li, X., and Pujari, L.: Seasonal responses of nutrient to hydrology
400   and biology in the southern Yellow Sea, Continental Shelf Research, 206, 104207, https://doi.org/10.1016/j.csr.2020.104207, 2020.

Guo, T., Li, K., Zhu, Y., Gao, H., and Yao, X.: Concentration and size distribution of particulate oxalate in marine and coastal atmospheres – Implication for the increased importance of oxalate in nanometer atmospheric particles, Atmospheric Environment, 142, 19–31, https://doi.org/10.1016/j.atmosenv.2016.07.026, 2016.

405   Hu, Q., Qu, K., Gao, H., Cui, Z., Gao, Y., and Yao, X.: Large increases in primary trimethylaminium and secondary dimethylaminium in atmospheric particles associated with cyclonic eddies in the northwest Pacific Ocean, Journal of Geophysical Research: Atmospheres, 123, 12,133-12,146, https://doi.org/10.1029/2018JD028836, 2018.

Hu, Q., Yu, P., Zhu, Y., Li, K., Gao, H., and Yao, X.: Concentration, size distribution, and formation of trimethylaminium and dimethylaminium ions in atmospheric particles over marginal seas of China, Journal of the Atmospheric Sciences,
410   72, 3487–3498, https://doi.org/10.1175/JAS-D-14-0393.1, 2015.

Jameson, E., Doxey, A. C., Airs, R., Purdy, K. J., Murrell, J. C., and Chen, Y.: Metagenomic data-mining reveals contrasting microbial populations responsible for trimethylamine formation in human gut and marine ecosystems, Microbial

Genomics, 2, https://doi.org/10.1099/mgen.0.000080, 2016.

Johnson, M. T., Liss, P. S., Bell, T. G., Lesworth, T. J., Baker, A. R., Hind, A. J., Jickells, T. D., Biswas, K. F., Woodward, E. M. S., and Gibb, S. W.: Field observations of the ocean-atmosphere exchange of ammonia: Fundamental importance of temperature as revealed by a comparison of high and low latitudes, Global Biogeochem. Cycles, 22, https://doi.org/10.1029/2007GB003039, 2008.

Keene, W. C., Long, M. S., Pszenny, A. A. P., Sander, R., Maben, J. R., Wall, A. J., O'Halloran, T. L., Kerkweg, A., Fischer, E. V., and Schrems, O.: Latitudinal variation in the multiphase chemical processing of inorganic halogens and related species over the eastern North and South Atlantic Oceans, Atmospheric Chemistry and Physics, 9, 7361–7385, https://doi.org/10.5194/acp-9-7361-2009, 2009.

Lidbury, I., Kimberley, G., Scanlan, D. J., Murrell, J. C., and Chen, Y.: Comparative genomics and mutagenesis analyses of choline metabolism in the marine Roseobacter clade, Environ Microbiol, 17, 5048–5062, https://doi.org/10.1111/1462-2920.12943, 2015a.

Lidbury, I. D., Murrell, J. C., and Chen, Y.: Trimethylamine and trimethylamine N-oxide are supplementary energy sources for a marine heterotrophic bacterium: Implications for marine carbon and nitrogen cycling, The ISME Journal, 9, 760–769, https://doi.org/10.1038/ismej.2014.149, 2015b.

Lutsch, E., Dammers, E., Conway, S., and Strong, K.: Long-range transport of NH3, CO, HCN, and C2H6 from the 2014 Canadian wildfires, Geophysical Research Letters, 43, 8286–8297, https://doi.org/10.1002/2016GL070114, 2016.

Mao, J., Yu, F., Zhang, Y., An, J., Wang, L., Zheng, J., Yao, L., Luo, G., Ma, W., Yu, Q., Huang, C., Li, L., and Chen, L.: High-resolution modeling of gaseous methylamines over a polluted region in China: source-dependent emissions and implications of spatial variations, Atmospheric Chemistry and Physics, 18, 7933–7950, https://doi.org/10.5194/acp-18-7933-2018, 2018

McNaughton, C. S., Clarke, A. D., Howell, S. G., Moore II, K. G., Brekhovskikh, V., Weber, R. J., Orsini, D. A., Covert, D. S., Buzorius, G., Brechtel, F. J., Carmichael, G. R., Tang, Y., Eisele, F. L., Mauldin, R. L., Bandy, A. R., Thornton, D. C., and Blomquist, B.: Spatial distribution and size evolution of particles in Asian outflow: Significance of primary and secondary aerosols during ACE-Asia and TRACE-P, Journal of Geophysical Research: Atmospheres, 109,

https://doi.org/10.1029/2003JD003528, 2004.

Müller, C., Iinuma, Y., Karstensen, J., van Pinxteren, D., Lehmann, S., Gnauk, T., and Herrmann, H.: Seasonal variation of aliphatic amines in marine sub-micrometer particles at the Cape Verde islands, Atmospheric Chemistry and Physics, 9, 9587–9597, https://doi.org/10.5194/acp-9-9587-2009, available at: https://acp.copernicus.org/articles/9/9587/2009/, 2009.

Pankow, J. F.: Phase considerations in the gas/particle partitioning of organic amines in the atmosphere, Atmospheric Environment, 122, 448–453, https://doi.org/10.1016/j.atmosenv.2015.09.056, 2015.

Paulot, F., Jacob, D. J., Johnson, M. T., Bell, T. G., Baker, A. R., Keene, W. C., Lima, I. D., Doney, S. C., and Stock, C. A.: Global oceanic emission of ammonia: Constraints from seawater and atmospheric observations, Global Biogeochem. Cycles, 29, 1165–1178, https://doi.org/10.1002/2015GB005106, 2015.

Prather, K. A., Bertram, T. H., Grassian, V. H., Deane, G. B., Stokes, M. D., Demott, P. J., Aluwihare, L. I., Palenik, B. P., Azam, F., Seinfeld, J. H., Moffet, R. C., Molina, M. J., Cappa, C. D., Geiger, F. M., Roberts, G. C., Russell, L. M., Ault, A. P., Baltrusaitis, J., Collins, D. B., Corrigan, C. E., Cuadra-Rodriguez, L. A., Ebben, C. J., Forestieri, S. D., Guasco, T. L., Hersey, S. P., Kim, M. J., Lambert, W. F., Modini, R. L., Mui, W., Pedler, B. E., Ruppel, M. J., Ryder, O. S., Schoepp, N. G., Sullivan, R. C., and Zhao, D.: Bringing the ocean into the laboratory to probe the chemical complexity of sea spray aerosol, Proc Natl Acad Sci U S A, 110, 7550–7555, https://doi.org/10.1073/pnas.1300262110, 2013.

Quinn, P. K., Collins, D. B., Grassian, V. H., Prather, K. A., and Bates, T. S.: Chemistry and related properties of freshly emitted sea spray aerosol, Chemical Reviews, 115, 4383–4399, https://doi.org/10.1021/cr500713g, 2015.

Quinn, P. K., Bates, T. S., Johnson, J. E., Covert, D. S., and Charlson, R. J.: Interactions between the sulfur and reduced nitrogen cycles over the central Pacific Ocean, J. Geophys. Res., 95, 16405–16416, https://doi.org/10.1029/JD095iD10p16405, 1990.

Sutton, M. A., Reis, S., Riddick, S. N., Dragosits, U., Nemitz, E., Theobald, M. R., Tang, Y. S., Braban, C. F., Vieno, M., Dore, A. J., Mitchell, R. F., Wanless, S., Daunt, F., Fowler, D., Blackall, T. D., Milford, C., Flechard, C. R., Loubet, B., Massad, R., Cellier, P., Personne, E., Coheur, P. F., Clarisse, L., van Damme, M., Ngadi, Y., Clerbaux, C., Skjøth, C. A., Geels, C., Hertel, O., Wichink Kruit, R. J., Pinder, R. W., Bash, J. O., Walker, J. T., Simpson, D., Horváth, L.,

Misselbrook, T. H., Bleeker, A., Dentener, F., and Vries, W. de: Towards a climate-dependent paradigm of ammonia emission and deposition, Philosophical Transactions of the Royal Society B: Biological Sciences, 368, 20130166, https://doi.org/10.1098/rstb.2013.0166, 2013.

Taubert, M., Grob, C., Howat, A. M., Burns, O. J., Pratscher, J., Jehmlich, N., Bergen, M. von, Richnow, H. H., Chen, Y., and Murrell, J. C.: Methylamine as a nitrogen source for microorganisms from a coastal marine environment, Environ Microbiol, 19, 2246–2257, https://doi.org/10.1111/1462-2920.13709, 2017.

Teng, X., Hu, Q., Zhang, L., Qi, J., Shi, J., Xie, H., Gao, H., and Yao, X.: Identification of major sources of atmospheric NH3 in an urban environment in northern China during wintertime, Environmental Science & Technology, 51, 6839– 6848, https://doi.org/10.1021/acs.est.7b00328, 2017.

Uematsu, M., Toratani, M., Kajino, M., Narita, Y., Senga, Y., and Kimoto, T.: Enhancement of primary productivity in the western North Pacific caused by the eruption of the Miyake-jima Volcano, Geophysical Research Letters, 31, https://doi.org/10.1029/2003GL018790, 2004.

van Pinxteren, M., Fomba, K. W., van Pinxteren, D., Triesch, N., Hoffmann, E. H., Cree, C. H.L., Fitzsimons, M. F., Tümpling, W. von, and Herrmann, H.: Aliphatic amines at the Cape Verde Atmospheric Observatory: Abundance, origins and sea-air fluxes, Atmospheric Environment, 203, 183–195, https://doi.org/10.1016/j.atmosenv.2019.02.011, 2019.

van Pinxteren, M., Fiedler, B., van Pinxteren, D., Iinuma, Y., Körtzinger, A., and Herrmann, H.: Chemical characterization of sub-micrometer aerosol particles in the tropical Atlantic Ocean: Marine and biomass burning influences, Journal of Atmospheric Chemistry, 72, 105–125, https://doi.org/10.1007/s10874-015-9307-3, 2015.

VandenBoer, T. C., Petroff, A., Markovic, M. Z., and Murphy, J. G.: Size distribution of alkyl amines in continental particulate matter and their online detection in the gas and particle phase, Atmospheric Chemistry and Physics, 11, 4319–4332, https://doi.org/10.5194/acp-11-4319-2011, 2011.

Wang, B., Chen, Y., Zhou, S., Li, H., Wang, F., and Yang, T.: The influence of terrestrial transport on visibility and aerosol properties over the coastal East China Sea, Science of The Total Environment, 649, 652–660, https://doi.org/10.1016/j.scitotenv.2018.08.312, 2019.

Wentworth, G. R., Murphy, J. G., Benedict, K. B., Bangs, E. J., and Collett Jr., J. L.: The role of dew as a night-time reservoir and morning source for atmospheric ammonia, Atmospheric Chemistry and Physics, 16, 7435–7449, https://doi.org/10.5194/acp-16-7435-2016, 2016.

490

Xie, H., Feng, L., Hu, Q., Zhu, Y., Gao, H., Gao, Y., and Yao, X.: Concentration and size distribution of water-extracted dimethylaminium and trimethylaminium in atmospheric particles during nine campaigns - Implications for sources, phase states and formation pathways, Science of The Total Environment, 631-632, 130–141, https://doi.org/10.1016/j.scitotenv.2018.02.303, 2018.

495

Yao, L., Garmash, O., Bianchi, F., Zheng, J., Yan, C., Kontkanen, J., Junninen, H., Mazon, S. B., Ehn, M., Paasonen, P., Sipilä, M., Wang, M., Wang, X., Xiao, S., Chen, H., Lu, Y., Zhang, B., Wang, D., Fu, Q., Geng, F., Li, L., Wang, H., Qiao, L., Yang, X., Chen, J., Kerminen, V.-M., Petäjä, T., Worsnop, D. R., Kulmala, M., and Wang, L.: Atmospheric new particle formation from sulfuric acid and amines in a Chinese megacity, Science, 361, 278–281, https://doi.org/10.1126/science.aao4839, 2018.

500

Yu, F., and Luo, G.: Modeling of gaseous methylamines in the global atmosphere: impacts of oxidation and aerosol uptake, Atmospheric Chemistry and Physics, 14, 12455–12464, https://doi.org/10.5194/acp-14-12455-2014, 2014

Yu, P., Hu, Q., Li, K., Zhu, Y., Liu, X., Gao, H., and Yao, X.: Characteristics of dimethylaminium and trimethylaminium in atmospheric particles ranging from supermicron to nanometer sizes over eutrophic marginal seas of China and oligotrophic open oceans, Science of The Total Environment, 572, 813–824,

505

https://doi.org/10.1016/j.scitotenv.2016.07.114, 2016.

Zhao, Y., Zhang, L., Pan, Y., Wang, Y., Paulot, F., and Henze, D. K.: Atmospheric nitrogen deposition to the northwestern Pacific: seasonal variation and source attribution, Atmospheric Chemistry and Physics, 15, 10905–10924, https://doi.org/10.5194/acp-15-10905-2015, 2015.

Zhou, S., Li, H., Yang, T., Chen, Y., Deng, C., Gao, Y., Chen, C., and Xu, J.: Characteristics and sources of aerosol

510

aminiums over the eastern coast of China: Insights from the integrated observations in a coastal city, adjacent island and surrounding marginal seas, Atmospheric Chemistry and Physics, 19, 10447–10467, https://doi.org/10.5194/acp-19-10447-2019, 2019.

Zhu, J., Shi, J., Guo, X., Gao, H., and Yao, X.: Air-sea heat flux control on the Yellow Sea Cold Water Mass intensity and implications for its prediction, Continental Shelf Research, 152, 14–26, https://doi.org/10.1016/j.csr.2017.10.006, 2018.

515 Zhu, Y., Li, K., Shen, Y., Gao, Y., Liu, X., Yu, Y., Gao, H., and Yao, X.: New particle formation in the marine atmosphere during seven cruise campaigns, Atmospheric Chemistry and Physics, 19, 89–113, https://doi.org/10.5194/acp-19-89-2019, 2019.
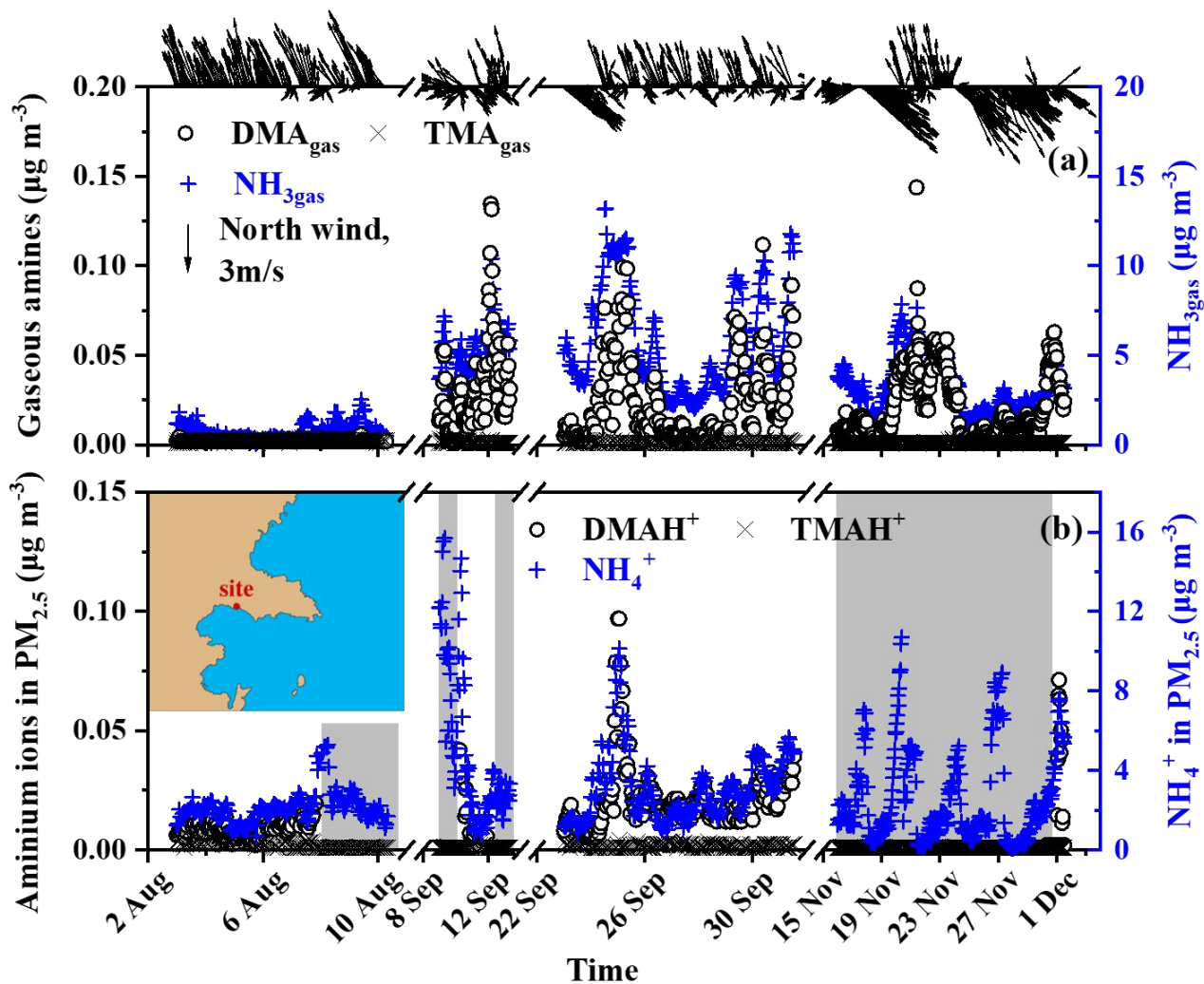
Figure 1: Temporal variations in the concentrations of NH_{3gas}, gaseous amines, and their counterparts in $PM_{2.5}$ at a coastal site during three seasons of 2019 ((a) NH_{3gas} and gaseous amines; (b) counterparts in $PM_{2.5}$; wind speed and direction superimposed on the top of (a); a map of the sampling site superimposed in (b); the missing data regarding aminium ions in the $PM_{2.5}$ shading in the gray shadow were due to occasional K^+ interference (b)).
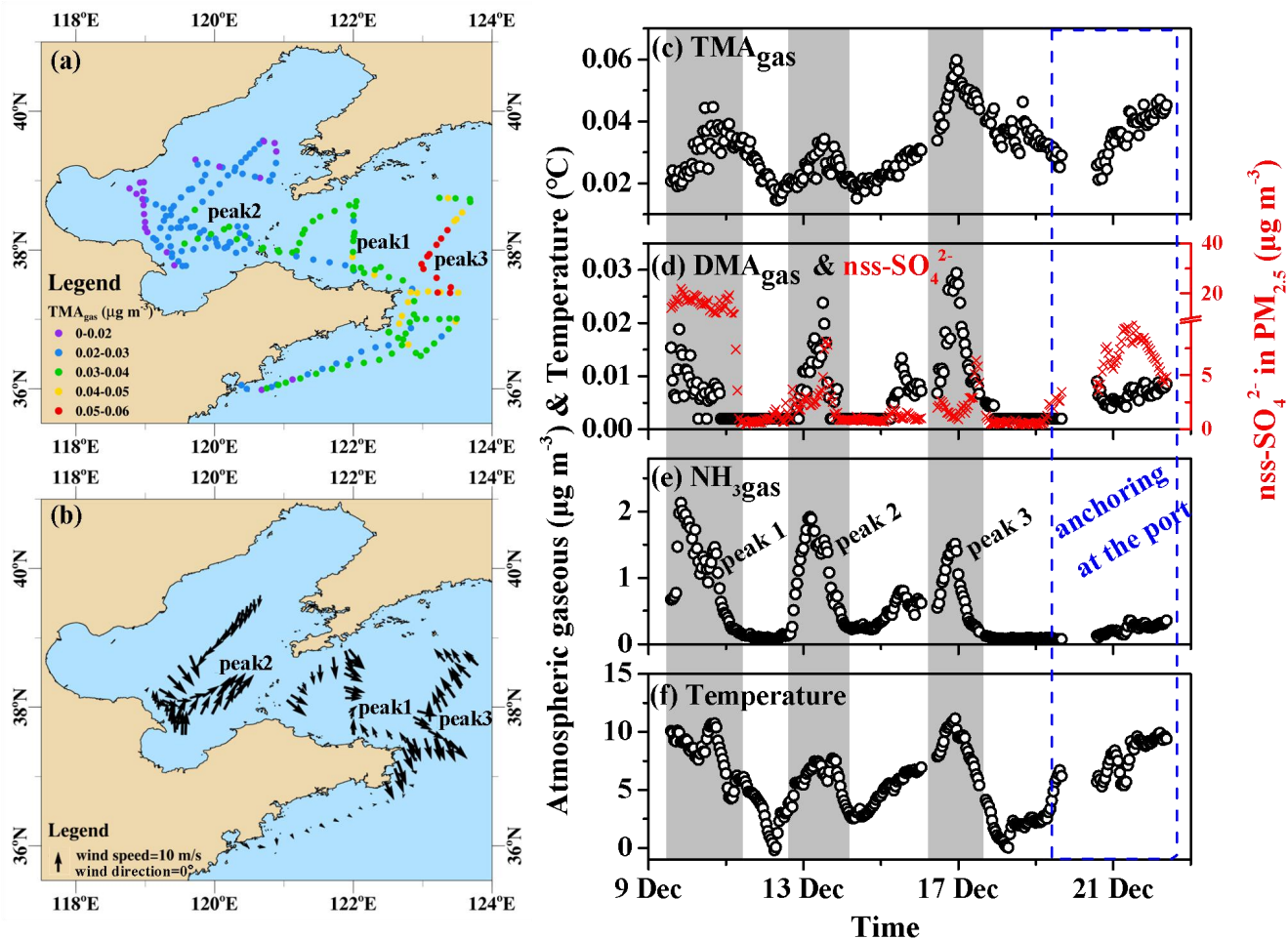
Figure 2: Spatiotemporal variations in the concentrations of basic gases and other parameters during cruise campaigns in the Yellow and Bohai seas on December 9-22, 2019 ((a) mapping TMA_{gas} by concentration; (b) mapping onboard recorded wind speeds and directions; time-series of (c) TMA_{gas}, (d) DMA_{gas}, (e) NH_{3gas}, and (f) ambient air temperature recorded onboard. The time-series of nss-SO_4^{2-} in $PM_{2.5}$ were shown as indicators of anthropogenic air pollutants in (d); not all data were shown in (b) to avoid clustering).
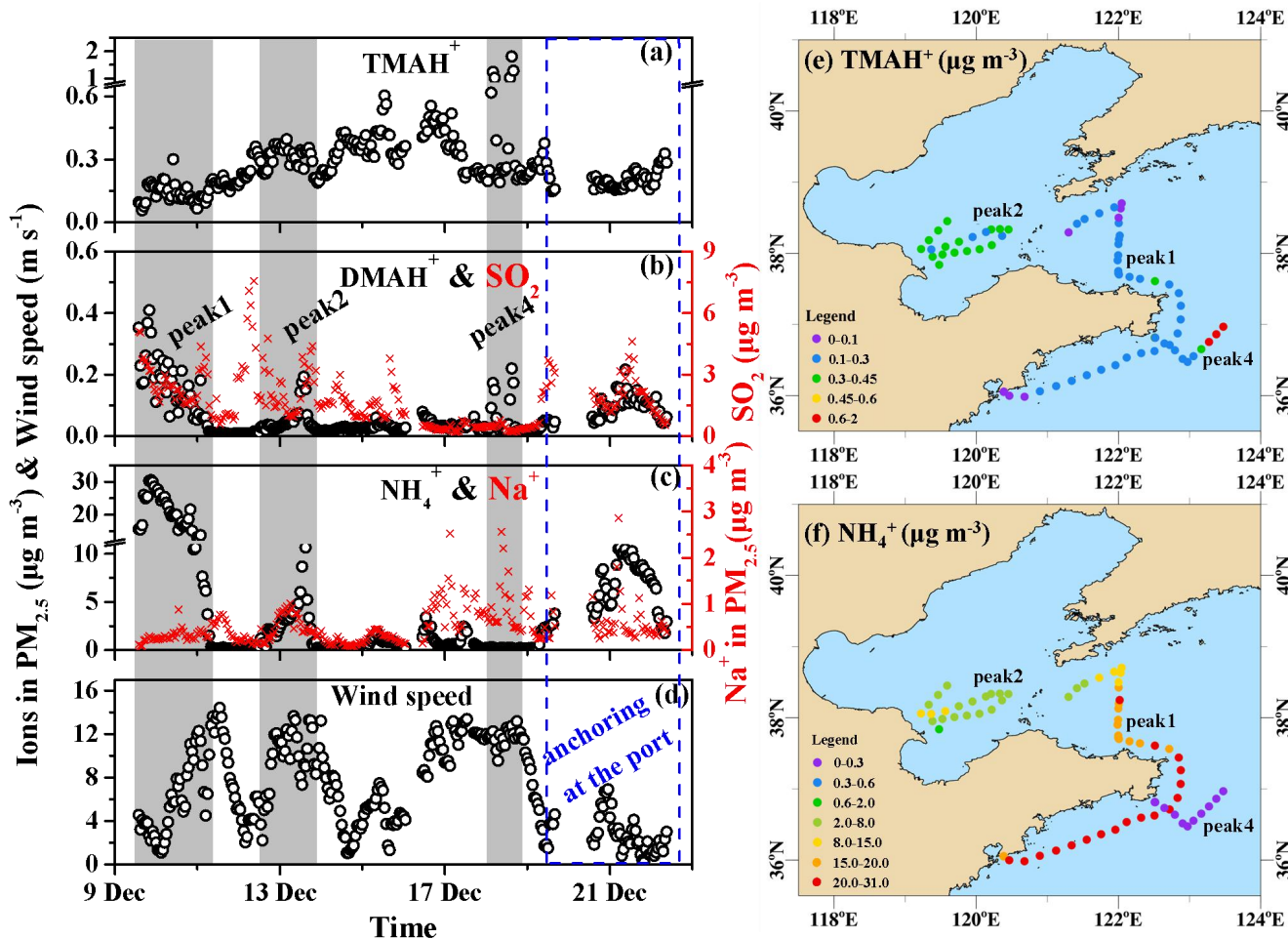
Figure 3: Spatiotemporal variations in the aminium ions and NH_4^+ concentrations of $PM_{2.5}$ and other parameters during cruise campaigns over the Yellow and Bohai seas on December 9-22, 2019 (time-series of (a) $TMAH^+$, (b) $DMAH^+$, and (c) NH_4^+ in $PM_{2.5}$; (d) wind speeds (WS); (e) mapping of the $TMAH^+$ in concentration; (f) mapping of the NH_4^+ concentration. The time-series of SO_2 is shown as an indicator in (b); that of Na^+ in $PM_{2.5}$ is shown as an indicator of sea-spray aerosols in (c). To better show the spatiotemporal distributions of $TMAH^+$ and NH_4^+ during peaks 1, 2, and 4, only the data during periods shaded in (a-d) were used in (e) and (f) to avoid clustering).

535
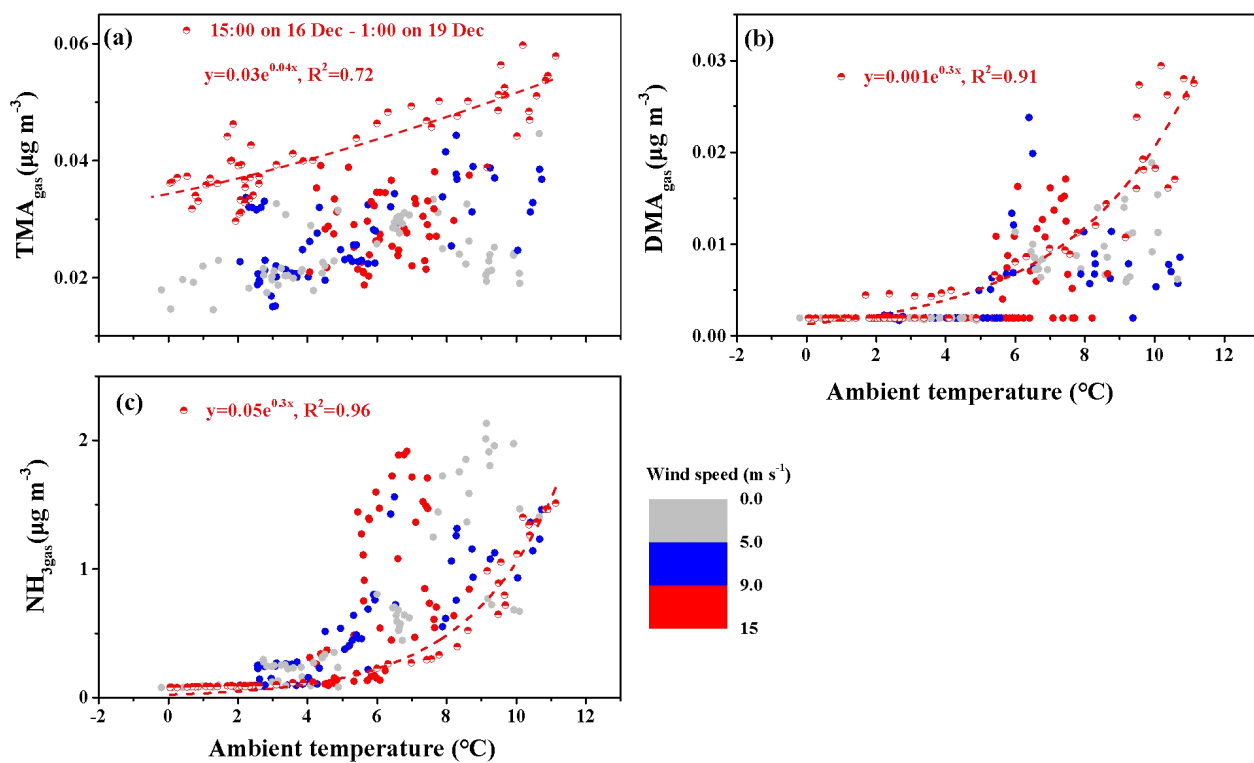
Figure 4: Correlations between the concentrations of basic gases and ambient temperature ((a) TMA$_{gas}$; (b) DMA$_{gas}$; (c) and NH$_3$. The colored bar represents different wind speeds; full symbols represent the data observed throughout the campaign excluding the period from 15:00 on December 16 to 01:00 on December 19, 2019).
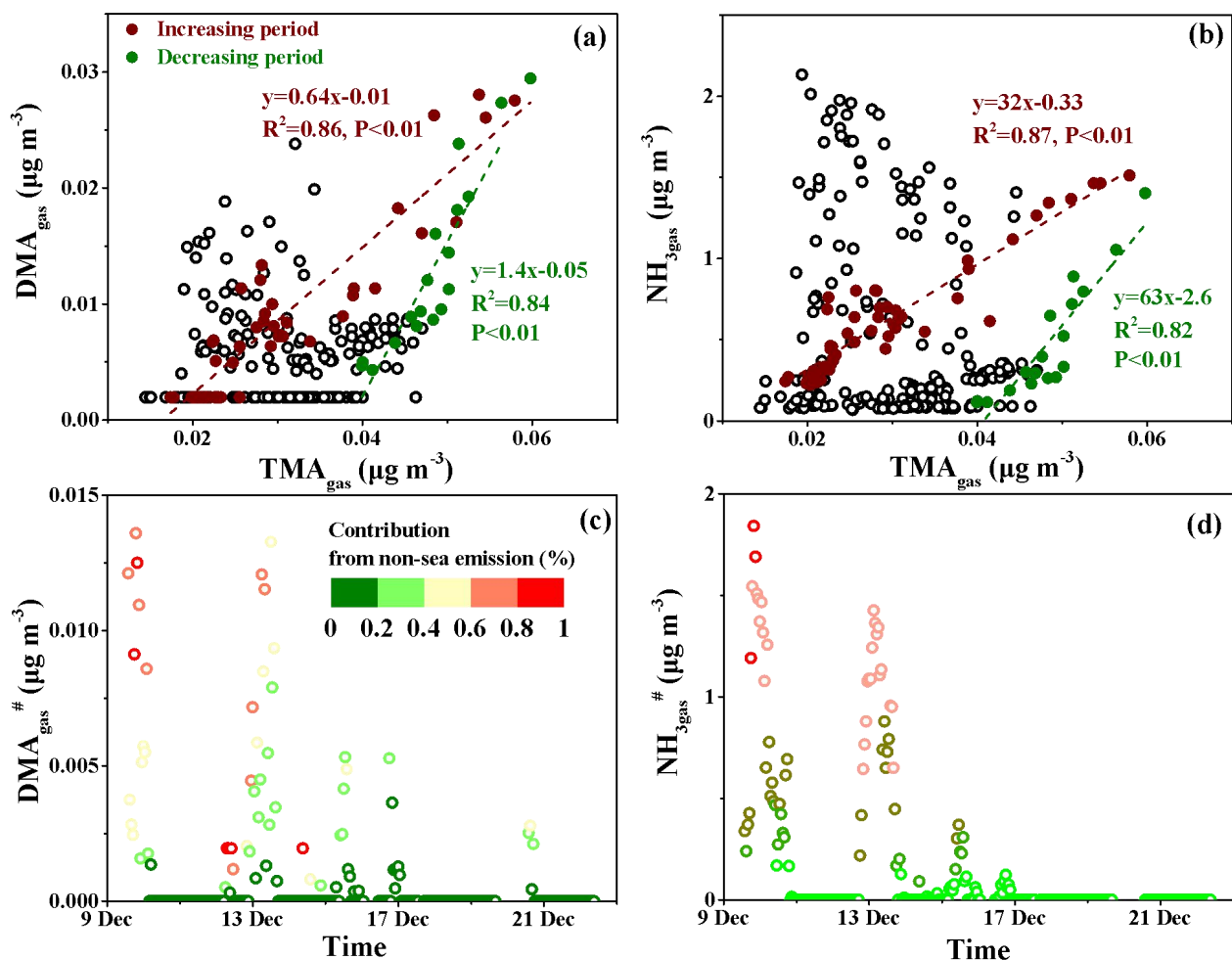
Figure 5: Correlations of DMA$_{gas}$ and NH$_{3gas}$ with TMA$_{gas}$ and time-series of the calculated DMA$_{gas}$# and NH$_{3gas}$# ((a) DMA$_{gas}$ vs. TMA$_{gas}$; (b) NH$_{3gas}$ vs. TMA$_{gas}$; (c) DMA$_{gas}$#; and (d) NH$_{3gas}$#. The colored bars in (c) and (d) represent the percentages of transported DMA$_{gas}$# and NH$_{3gas}$# in each corresponding observed value).

545
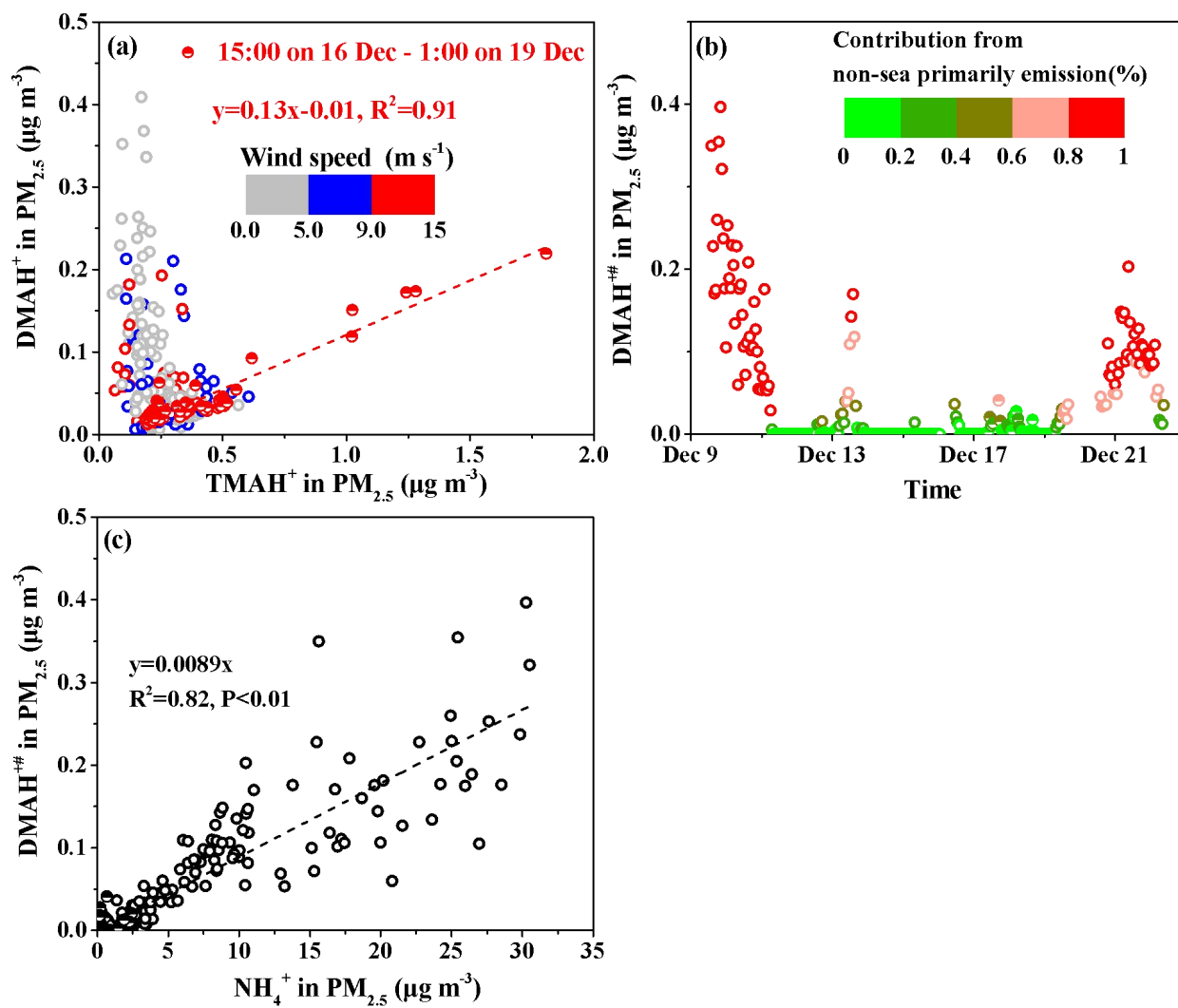
Figure 6: Correlation analyses of different variables in PM$_{2.5}$ and the time-series of the calculated DMAH$^{+\#}$ in PM$_{2.5}$ ((a) DMAH$^+$ vs. TMAH$^+$; (b) time-series of DMAH$^{+\#}$; (c) DMAH$^{+\#}$ vs. NH$_4^+$).